Science Bulletin xxx (xxxx) xxx

Contents lists available at ScienceDirect

Science Bulletin

journal homepage: www.elsevier.com/locate/scib

Article

Global mapping of urban thermal anisotropy reveals substantial potential biases for remotely sensed urban climates

Huilin Du [a], Wenfeng Zhan [a,b,*], Zihan Liu [a,*], E. Scott Krayenhoff [c], TC Chakraborty [d], Lei Zhao [e], Lu Jiang [a], Pan Dong [a], Long Li [a], Fan Huang [a], Shasha Wang [a], Yuyue Xu [f]

[a] Jiangsu Provincial Key Laboratory of Geographic Information Science and Technology, International Institute for Earth System Science, Nanjing University, Nanjing 210023, China
[b] Jiangsu Center for Collaborative Innovation in Geographical Information Resource Development and Application, Nanjing 210023, China
[c] School of Environmental Sciences, University of Guelph, Guelph N1G 2W1, Canada
[d] Atmospheric Sciences and Global Change Division, Pacific Northwest National Laboratory, Richland 99352, USA
[e] Department of Civil and Environmental Engineering, University of Illinois at Urbana-Champaign, Urbana 61820, USA
[f] School of Geography and Ocean Science, Nanjing University, Nanjing 210023, China

ARTICLE INFO

Article history:
Received 1 December 2022
Received in revised form 26 April 2023
Accepted 27 April 2023
Available online xxxx

Keywords:
Thermal remote sensing
Urban thermal anisotropy
Global urban climates
Urban surface fluxes
Urban heat island

ABSTRACT

Urban thermal anisotropy (UTA) drastically impacts satellite-derived urban surface temperatures and fluxes, and consequently makes it difficult to gain a more comprehensive understanding of global urban climates. However, UTA patterns and associated biases in observed urban climate variables have not been investigated across an adequate number of global cities with diverse contexts; nor is it known whether there are globally measurable factors that are closely related to the UTA intensity (UTAI, quantified as the maximum difference between the nadir and off-nadir urban thermal radiation). Here we investigate the UTAI over more than 5500 cities worldwide using multi-angle land surface temperature (LST) observations from 2003 to 2021 provided by Moderate Resolution Imaging Spectroradiometer (MODIS). The results show that the global mean UTAI can reach 5.1, 2.7, 2.4, and 1.7 K during summer daytime, winter daytime, summer nighttime, and winter nighttime, respectively. Using nadir LST observations as a reference, our analysis reveals that UTA can lead to an underestimation of satellite-based urban surface sensible heat fluxes (H) by 45.4% and surface urban heat island intensity (I_s) by 43.0% when using LST observations obtained from sensor viewing zenith angles (VZAs) of ±60°. Practitioners can limit the biases of H and I_s within ±10% by using LSTs from sensor VZAs within ±30°. We also find that UTAI is closely related to urban impervious surface percentage and surface air temperature across global cities. These findings have implications for angular normalization of satellite-retrieved instantaneous LST observations across cities worldwide.

1. Introduction

An in-depth understanding of urban climates across global cities is critical for designing appropriate adaptation strategies to address urban-scale climate impacts [1–4]. Traditional urban climate studies mostly rely on *in-situ* measurements obtained from weather stations sparsely distributed within cities [5,6]. These sparsely distributed urban measurement networks, nevertheless, are usually unable to provide adequate spatial details of complex and highly heterogeneous urban environments [7], especially across global cities. Satellite thermal remote sensing can provide spatially consistent observations over large scales [8–10] and has been extensively used in urban climate studies (especially for urban surface energy budget and surface urban heat island, SUHI) in the last two decades [11–15]. However, cities are characterized by notable urban thermal anisotropy (UTA) [16], a common phenomenon in which the thermal emissions of urban surfaces are directionally dependent (Fig. 1). The UTA intensity (UTAI), defined as the difference between maximum and minimum thermal radiation or the maximum difference between nadir and off-nadir thermal radiation, can reach 10.0 K or more over typical urban surfaces [17]. The UTA substantially distorts satellite-based analyses of urban climates [18] and severely limits the in-depth understanding of global urban climates as well as the design of appropriate urban climate adaptation strategies [19,20].

To better understand UTA, its associated impacts, and relevant factors, studies have employed various strategies (e.g., computer

* Corresponding authors.
E-mail addresses: zhanwenfeng@nju.edu.cn (W. Zhan), liuzihan_trs@foxmail.com (Z. Liu).

https://doi.org/10.1016/j.scib.2023.06.032

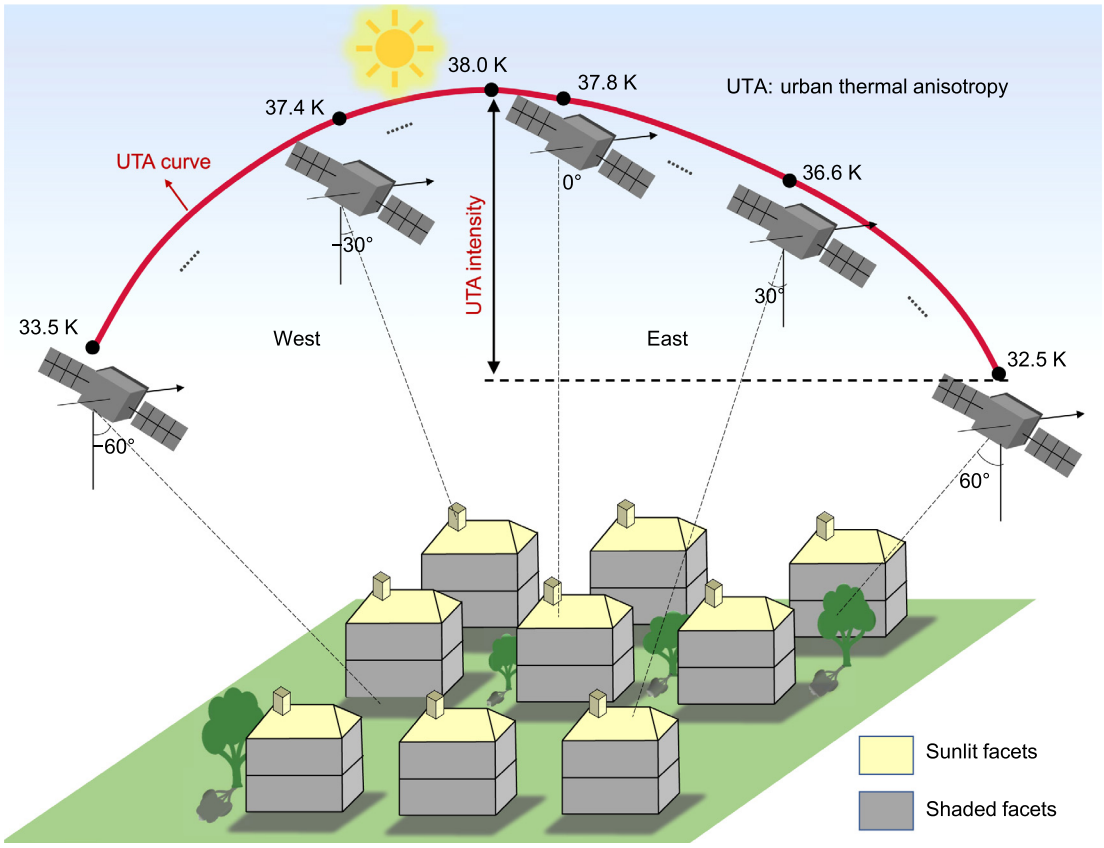

Fig. 1. Illustration of urban thermal anisotropy (UTA). The angle (°) denotes the sensor viewing zenith angle (VZA), with positive and negative values representing observations from the east and west directions, respectively. The temperature (K) signifies the satellite-derived land surface temperature (LST) for a certain sensor VZA. The sunlit urban components (yellow color) usually possess higher LSTs while the shaded (grey color) typically have relatively lower ones.

simulations and airborne and spaceborne observations) to examine the UTA, mostly over a few selected cities [18,21–25]. These previous studies all confirm that the UTAI is usually higher during the day than at night [18,26], while seasonal UTAI variations are still under debate—some findings suggest a stronger UTAI in summer than in winter [25,27], yet others indicate a larger UTAI in winter [22]. The UTA can notably bias the estimation of urban climate variables. For example, the UTA-induced bias in surface longwave radiation flux of Sapporo and Tokyo in Japan can reach 8% [23]; the UTA-induced bias in surface sensible heat flux was found to be up to 15%–40% concluded from a low-rise industrial area of Vancouver, Canada [24]; and the bias in SUHI intensity can account for 25%–50% of the overall observed SUHI intensity of New York and Chicago in the United States [18]. In terms of the UTA-related factors, the UTAI has been shown to be regulated by urban geometry, sun-surface-sensor geometric configuration, surface thermal properties, and background climate (or weather) conditions [25,28,29].

Although significant progress has been made, most previous approaches for identifying UTA often require detailed surface or atmospheric information and they are very difficult to be extended to a large scale. A recent study has overcome the necessity of proximate water body references required in previous literatures, but it is also limited to a relatively small number of cities worldwide [25]. Therefore, the UTA pattern across an adequate number of global cities with diverse contexts and its induced biases in urban climate variables remain largely unknown. In addition, it remains unclear whether there are globally acquirable factors that are closely related to UTAI and can be used for UTA correction. Here we aim to answer the following three questions related to global UTA: (1) what are the spatiotemporal UTA patterns across global cities? (2) How does UTA affect the remotely sensed estimates of global urban surface energy fluxes and SUHI intensity? (3) How are the global UTAI related to the commonly used surface and atmospheric variables? To address these issues, we combine all multi-angle MODIS LST observations (2003–2021) with the Google cloud computing platform and examine the spatiotemporal UTA patterns over more than 5500 cities worldwide. We further investigate the UTA-induced biases in the estimation of several key urban surface energy flux components and SUHI intensity (i.e., added warmth of urban surfaces relative to rural surroundings). We finally analyze the relationships between the UTAI and several factors that strongly regulate the UTAI and are easily acquirable on a global scale. Our results provide a deeper fundamental understanding of global UTA and can promote the remote sensing of global urban climates.

2. Materials and methods

2.1. Study area and data

We chose a total of 5586 cities (each with an urban area larger than 10 km^2 in the year 2000) worldwide (Fig. S1 online). We employed MODIS products, a reanalysis dataset, and other auxiliary data to assist analysis. The MODIS products include daily LST (MYD11A1 and MOD11A1 V6 products; with a spatial resolution of 1 km; [30]), yearly land cover type (MCD12Q1 V6 product; 500 m; [31]), and 16-day composite enhanced vegetation index (EVI; MOD13A2 V6 product; 1 km; [32]). The ERA5-land reanalysis dataset (11 km; [33]) used here provides hourly surface air temperature (SAT) and downward shortwave radiation (RAD). Auxiliary data include global urban boundary (GUB; [34]), global impervious surface percentage (ISP; 38 m; [35]), and building

height information for Europe, the United States, and China (1 km; [36]). More descriptions on the study area and data usage are provided in Note S1 (online).

2.2. Calculation and investigation of UTAI across global cities

We developed a systematic approach to quantify the UTAI across global cities. This approach involves four steps, including the selection of clear-sky pixels, the division of MODIS sensor VZA groups, the calculation of LST for each VZA group, and the depiction of UTA curve (see Note S2 online). We then calculated the UTAI as the maximum difference between the nadir and off-nadir LSTs [17,25]. We acknowledge that the threshold setting in the UTAI calculation may bias the UTAI quantification, and that the inclusion of LST observations over a relatively long period (18 years) may also distort the results due to urbanization-induced land cover changes. We therefore performed a sensitivity analysis to demonstrate the low sensitivity of our results to the threshold setting (see Note S2 online). Besides, the global UTAI quantification may also be biased by several potential uncertainties induced by daily weather variations and residual atmospheric effects that impact the MODIS LST products. We therefore further discussed these two possible uncertainties and compared our results with those quantified by Ref. [18] in New York and Chicago, and with those quantified by Ref. [25] in 25 global cities to test the robustness of our proposed approach (see Note S3 online). Note that this study did not consider the impacts from topography on global UTAI quantification, mainly due to the relatively small elevation variation within most cities (Fig. S2a online). However, to demonstrate the robustness of our results, we further calculated the UTAI across global cities using only pixels with elevations within ±50 m of the median elevation of urban pixels (Fig. S2b online).

We separated our global UTAI analysis by climate zones and latitudes, and examined diurnal and seasonal variations to contextualize these results within corresponding patterns seen for urban climate using satellite-derived LST [8]. For cities in the Northern Hemisphere, we defined summer as June to August and winter as December to February, and *vice versa* for cities in the Southern Hemisphere. Due to the different LST missing rates in different seasons, the chosen cities may be inconsistent at different observation times (Table S1 online; the relative representation of cities across various continents was provided in Fig. S3 online). However, these slight inconsistencies of city number among different observation times should not invalidate the main findings due to the relatively large sample size (mostly greater than 4000 cities) [37] as well as the relatively uniform distribution of the available cities worldwide (Fig. S4 online).

2.3. Quantification of UTA-induced biases in typical urban climate variables across global cities

Satellite thermal remote sensing serves as the only plausible means to estimate, at the global scale, a series of urban climate variables including the urban surface energy fluxes (i.e., surface-emitted longwave radiation, sensible heat flux, latent heat flux, and Bowen ratio, termed *E*, *H*, *LE*, and *BR*, respectively) and the SUHI intensity (termed I_s) [6,8,9]. The notable UTA can drastically distort the estimation of these urban climate variables. We investigated the UTA-induced biases in the estimates of these variables across global cities. Specifically, we took the values calculated based on the nadir LST observations as references and quantified the bias for each sensor VZA as the difference from this reference nadir estimate. We further calculated the UTA-induced biases in percentages as the ratio of the bias to the reference value. For the I_s calculation, we delineated the rural surroundings as the ring areas between the 10- and 50-km buffer zones outside the corresponding urban areas (Fig. S5 online; [38]). The pixels beyond ±50 m of the median elevation of each city and those identified as "urban and built-up" according to the land cover type products were further disregarded to delineate the rural surfaces more reasonably. We calculated the I_s for a certain sensor VZA as the mean LST difference between all available urban and rural pixels [18]. The calculations of the percentage biases in *E*, *LE*, *H*, *BR*, and I_s are detailed in Note S4 (online).

2.4. Examination of relationships between UTAI and several globally available surface and atmospheric factors

The city-scale UTAI has been shown to be strongly regulated by urban form such as aspect ratio and weather conditions such as RAD and SAT [18,25,26,29,39,40]. However, aspect ratio information is extremely difficult to obtain for thousands of cities worldwide. In contrast, urban ISP is globally available [41] and is also highly correlated with aspect ratio [18]. We therefore mainly chose ISP to analyze the relationships between UTAI and urban form across global cities. For each city, we divided its urban surfaces into 10 categories according to the ISP values, and investigated the UTAI variations with ISP. Cities with ISP values greater than 80% at the 1-km scale are relatively limited in number and unevenly distributed around the world. We therefore did not include the ISP category of >80% in the analysis. We further analyzed the relationships between UTAI and EVI across global cities, mainly because of the high negative correlation between EVI and ISP [42]. We also examined the relationships between UTAI and building height, but only in regions where these data were available, i.e., Europe, the United States, and China.

We further analyzed the relationships between UTAI and two atmospheric indicators, namely SAT and RAD across global cities (Fig. S6 online). Since the analyses between UTAI and both SAT and RAD are similar, we describe the procedures for SAT only. Considering that SATs in neighboring cities within the same climate zone are usually close [33], we first divided the global cities into 244 urban agglomerations by each 15°×15° grid and climate zone. For each urban agglomeration, we first converted the reanalysis SAT products, which are in coordinated universal time (UTC), to local solar time according to the located time zone of the urban agglomeration to match the MODIS LST products. We then calculated the mean SAT over a 5-h period around the satellite transit times and classified the SATs into 20 groups in ascending order within each season, with each SAT group representing different weather conditions. We further extracted the LST observations under each SAT condition by matching the dates (i.e., year-month-day) of SAT and LST, obtaining a total of 20 LST groups. We then calculated the UTAI using all LST groups for each urban agglomeration and analyzed the relationships between UTAI and SAT across global cities. Here we employed the mean SAT over a 5-h period around the satellite transit times (e.g., the SAT averaged between 10:00 am and 15:00 pm local solar time was used for the Aqua-based daytime UTAI analysis), mainly because satellite transit times for the same area can vary by about 2 h on different days (Fig. S7 online). Besides, weather conditions during several hours before the satellite transit could also strongly modulate the UTAI due to the influence of thermal inertia [26], we therefore also included the RAD of 2 h before the satellite transit times. Similarly, the SAT category without an adequate number of cities would not be considered. To better characterize the relationships between UTAI and both the surface and atmospheric factors, we further examined the UTAI variations along with both ISP and SAT over global cities.

3. Results and discussion

3.1. Spatiotemporal UTA pattern across global cities

We quantified the UTAI using all available MODIS LST observations between 2003 and 2021 and analyzed the spatiotemporal UTA patterns over more than 5500 cities worldwide. The results confirm that cities worldwide are characterized by strong UTA, and the UTA curve demonstrates a notable hotspot effect (Fig. 2). Around 10:30 local solar time (transit time of the Terra satellite) when the sun is on the eastern side, the zenith angle of the hotspot ranges between +5° and +15° (with the eastern direction defined as positive; Fig. 2c). Similarly, the hotspot is oriented towards the sun (i.e., west) around 13:30 (transit time of the Aqua satellite; Fig. 2c).

Across global cities, the maximum difference between the nadir and off-nadir LST differences (i.e., the UTAI) exhibits a high diurnal variation (Fig. 2d and Fig. S4 online). The UTAI during the day is approximately twice as high as that at night. The global mean daytime UTAI are 3.7 K (i.e., averaged for summer and winter, and similarly below) and 4.2 K around 10:30 and 13:30, respectively, while the global mean nighttime UTAI are only 2.2 and 1.9 K for 22:30 and 01:30, respectively (Fig. 2d). Strong solar radiation during the daytime; and consequently the larger LST differences among urban facets contribute to such a day-night UTAI contrast [17]. The global UTAI is also characterized by evident seasonal variations (Fig. 2d; Figs. S4 and S8 online). The largest global UTAI occurs in summer during both daytime and nighttime, followed by spring and autumn; and the global UTAI reaches its minimum in winter (Fig. S8 online). The summertime UTAI (3.7 K, averaged for daytime and nighttime, and similarly below) is about 1.6 times larger than the wintertime one (2.3 K). In a portion of the mid- or high-latitude cities in the northern hemisphere, however, the daytime UTAI is larger in winter than in summer (Fig. S4a–d online). By referring to previous case studies based on model simulations [22,43,44],

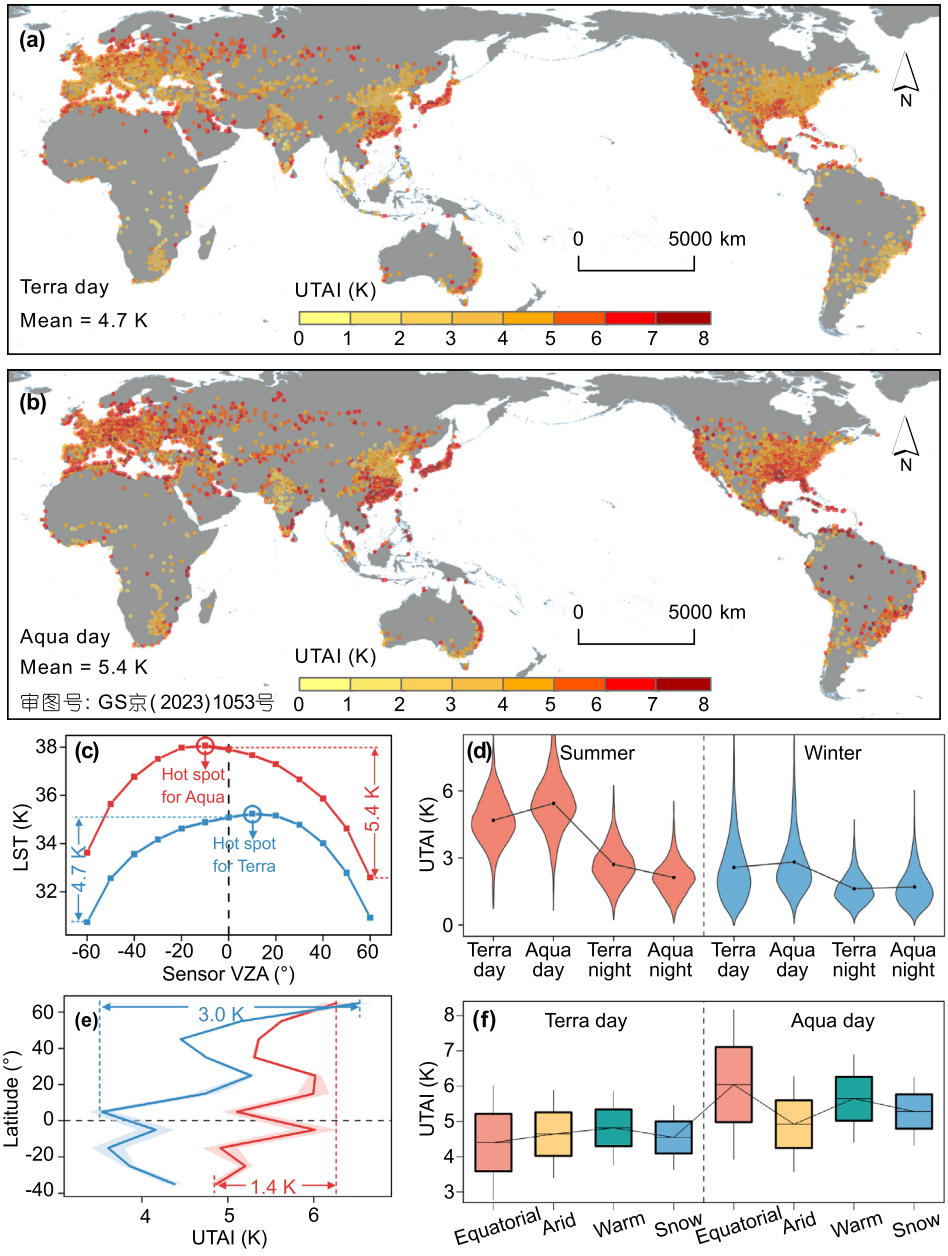

Fig. 2. Spatiotemporal UTA pattern across global cities. The city-by-city UTAI at around ~10:30 (a) and 13:30 (b) during summer daytime; the global mean UTA curve for these two times within a diurnal cycle (c); the diurnal and seasonal UTAI variations across global cities (d); and the UTAI averaged for cities at different latitudes (e) and across different climate zones (f).

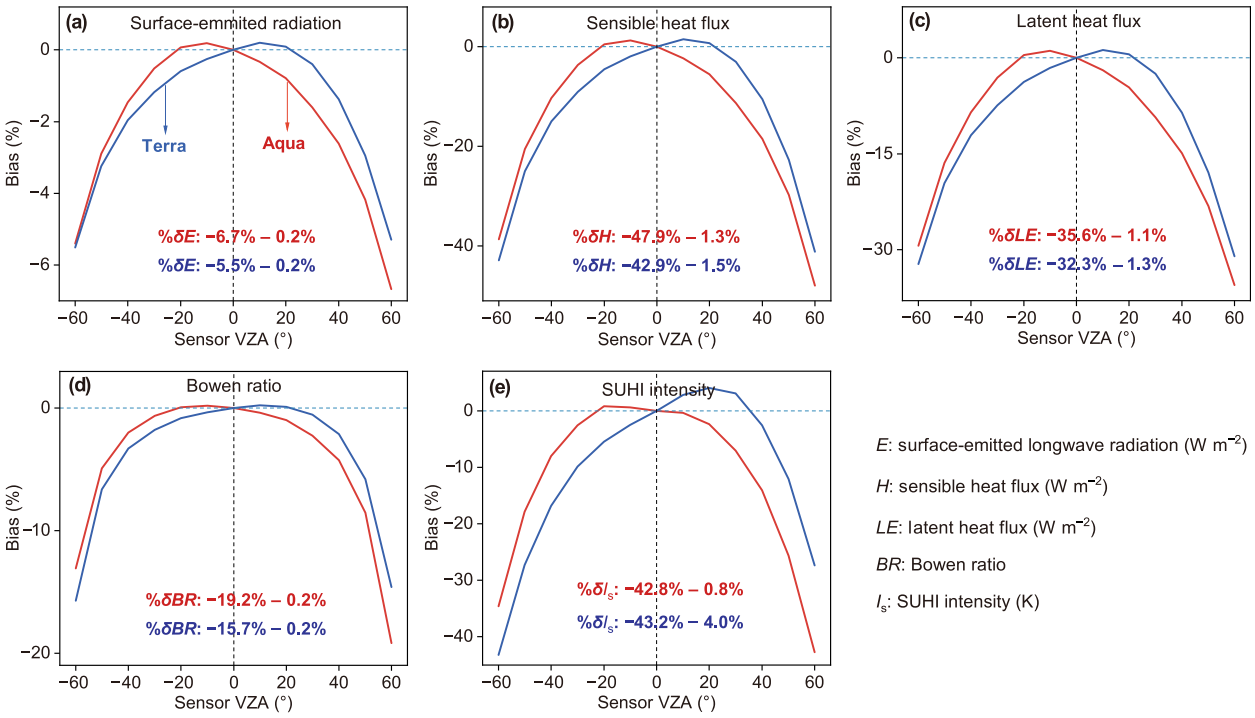

Fig. 3. UTA-induced biases in remotely sensed estimations of urban surface energy fluxes and SUHI intensity during summer daytime across global cities. UTA-induced biases in surface-emitted radiation flux (*E*) (a), sensible heat flux (*H*) (b), latent heat flux (*LE*) (c), Bowen ratio (*BR*) (d), and SUHI intensity (I_s) (e).

we speculate that the significantly larger winter UTAI over this region may be due to the combined effects of solar radiation, sun position, urban geometry (e.g., building orientation), and LST retrieval procedures. However, future endeavors are still needed to further unravel the underlying mechanism of this phenomenon through a combination of model simulations and exploration of the intrinsic retrieval processes of MODIS LSTs. Note that our quantified UTAI values are slightly larger than those reported in Ref. [25] across 25 global cities during both summer and winter (Fig. S9 online). The patterns of UTA curves are in good agreements with Ref. [25] during summer; however, a distinct difference is observed during winter. These disparities in the magnitudes and curves could be largely attributed to the different methods used to eliminate daily weather variabilities in each study (refer to Note S3 online). Additionally, we speculate that the small UTAI magnitude and poor quality of LST observations during winter may also introduce potential uncertainties into UTAI quantification, leading to the notable differences between these two studies for wintertime.

The UTAI also varies with latitude (Fig. 2e and Fig. S10 online). In the morning (i.e., ~10:30), the mean UTAI for mid- and high-latitude cities is considerably larger than that for low-latitude cities, characterized by a latitudinal variation of 3.0 K (Fig. 2a, e). By contrast, the latitudinal UTAI variation is less pronounced in the afternoon (i.e., ~13:30; Fig. 2b, e). The UTAI also differs by climate zone (Fig. 2f). The UTAI rarely changes along with climate zone in the morning. In the afternoon, however, the maximum UTAI occurs in equatorial climate (6.0 K), followed by warm climate (5.6 K) and snow climate (5.3 K). The smallest UTAI occurs in arid zone (4.9 K). Such regional discrepancies could be associated with the differences in urban form and the relative sun-sensor position [29].

3.2. UTA-induced biases in remotely sensed urban climate variables across global cities

We quantified the UTA-induced biases in satellite-retrieved urban climate variables for summer daytime across global cities, using nadir LST observations as references. The results show that urban surface fluxes can be substantially underestimated when using satellite-derived LSTs obtained at a specific zenith angle (Fig. 3). The UTA-induced bias in surface-emitted longwave radiation (*E*) ranges from −6.1% to 0.2% (Fig. 3a). The biases in urban sensible heat flux (*H*), latent heat flux (*LE*), and Bowen-ratio (*BR*) are considerably larger—the bias in *H* ranges from −45.4% to 1.4% (Fig. 3b), that in *LE* ranges from −34.0% to 1.2% (Fig. 3c), and that in *BR* ranges from −17.5% to 0.2% (Fig. 3d). To quantify the UTA-induced bias in SUHI intensity (I_s), we also quantified the thermal anisotropy of the rural surroundings of global cities. Our results show that the global mean thermal anisotropy intensity of the rural surroundings can reach 3.9 K during summer daytime (Fig. S11 online; averaged for Aqua- and Terra-based results). This means that the absolute values of urban temperature, which are often more relevant for practical purposes [45], can suffer from much larger thermal anisotropy-induced biases compared to their rural surroundings (i.e., 5.1 K versus 3.9 K; Fig. S11 online). The understandably weaker intensity over rural surroundings when compared with that of global urban surfaces may be due to the lower heterogeneity of rural surfaces. This suggests that the possible thermal anisotropy induced bias in I_s is approximately 1.2 K (i.e., 5.1 K minus 3.9 K). Although this value is not large and the thermal anisotropy effect can be largely offset by subtracting urban and rural LSTs, it can produce a relatively large bias in I_s (−43.0%–2.4%; Fig. 3e), since the global mean I_s during summer daytime is only 2.8 K (Fig. S11 online). More importantly, thermal anisotropy-induced biases in I_s can be greater than 50% in approximately 39% of global cities (Fig. 4). From a climatic perspective, thermal anisotropy generally underestimates the I_s in equatorial, warm, and snow climate zones, while it can lead to an overestimation of I_s in arid climate zone (Fig. S12 online). This difference between climate zones is particularly pronounced in North American cities, where UTA can significantly overestimate the I_s of dry cities and underestimate the I_s of humid cities (Fig. 4 and Fig. S13 online).

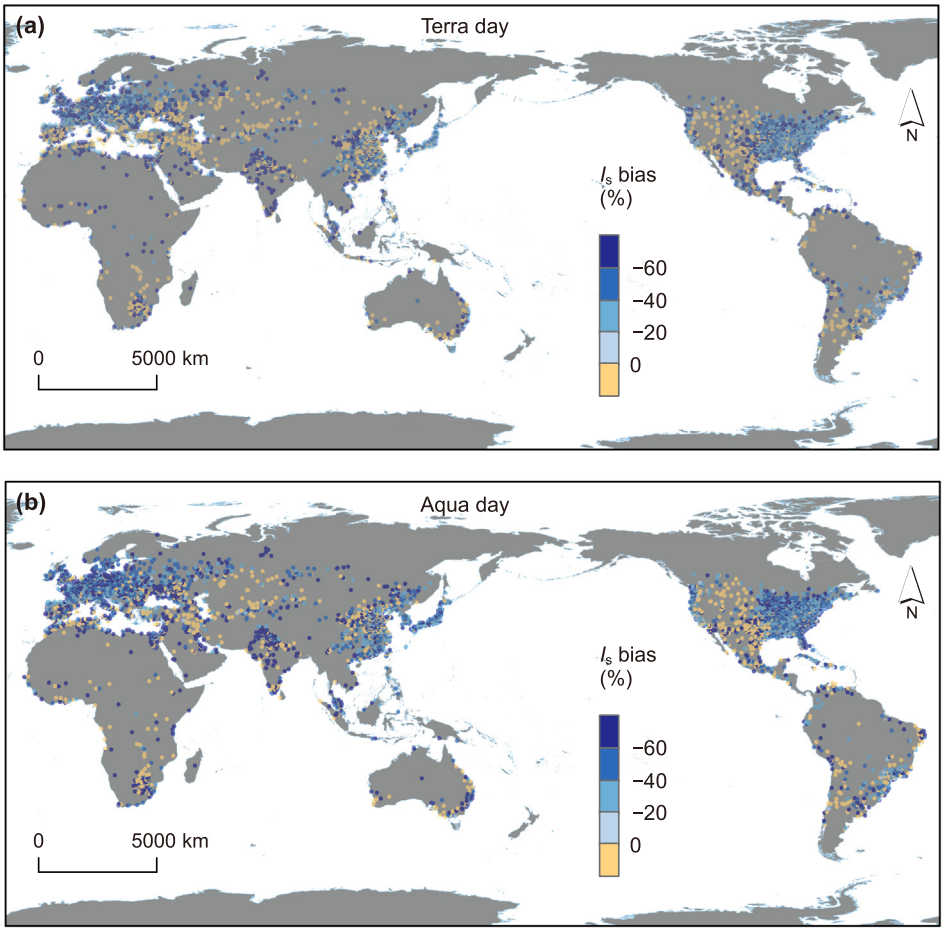

Fig. 4. Thermal anisotropy-induced biases in SUHI intensity (also termed I_s) across global cities during summer daytime for Terra (a) and Aqua (b).

3.3. Relationships between UTAI and globally acquirable surface and atmospheric factors

We further investigated the statistical relationships between the global UTAI and three globally acquirable surface factors, namely urban ISP, EVI, and building height, and two atmospheric factors, namely SAT and RAD. The analysis shows that the UTAI generally increases with urban ISP across global cities (Fig. 5a–c and Fig. S14 online). Specifically, the global mean UTAI increases from 4.3 K over low density urban surfaces (0 < ISP < 10%) to 5.5 K over highly urbanized surfaces (70% < ISP < 80%). Urban surfaces with high ISP are usually close to the city core and tend to possess larger aspect ratios, which can result in a larger LST difference among urban surface components and therefore a greater UTAI [18,29]. Across global cities, the UTAI first increases and then decreases with urban EVI, with the EVI inflection point occurring at 0.13 (Fig. 6a–c). The first increase in UTAI with EVI may be due to that tree canopies are typically taller than buildings over low EVI surfaces, creating a larger proportion of cool surfaces by casting more shadows and thereby enhancing UTAI [44]. Further investigation reveals that the UTAI also increases with urban building height, but in a nonlinear fashion. The UTAI increases steadily from 4.7 to 5.2 K when building height rises from 3 to 11 m, while it grows by less than 0.1 K when building height rises from 11 to 23 m (Fig. 6d–f). These findings are in good agreements with model-based results [29]. The shaded surfaces visible to the sensor would not increase much beyond a certain point as the buildings get taller due to occlusion effect, which may contribute to a relatively constant LST difference among urban facets and thus a stable UTAI.

Across global cities, the UTAI generally increases with SAT (Fig. 5d–f). Around 10:30, the UTAI increases from 4.3 to 5.6 K when SAT increases from 16 to 30 °C. Around 13:30, the UTAI first increases when SAT rises from 17 to 29 °C and then decreases slightly when SAT grows from 29 to 34 °C. The systematic UTAI difference between equatorial and other climate zones may contribute to the relatively high UTAI at 29 °C (Fig. S14d online). Consistent with previous modeling results [26,29], our analysis does confirm that the UTAI is positively correlated with RAD, yet we find that the UTAI variation along with RAD is much smaller than that with SAT on a global scale (Fig. S6 online). We speculate that the slightly weaker correlation between global UTAI and RAD may be associated with the inherent limitations in the used RAD product. These results reveal that ISP and SAT may act as surrogates for more direct controls of UTAI on a global scale, yet model-based simulations remain necessary to further verify these findings. We further analyzed the UTAI variations jointly regulated by ISP and SAT. The assessments imply a significant relationship between the UTAI and the two factors including ISP and SAT (Fig. 5g, h). These relationships can help assist the angular normalization of satellite-derived urban LSTs obtained at off-nadir angles (see Section 3.4).

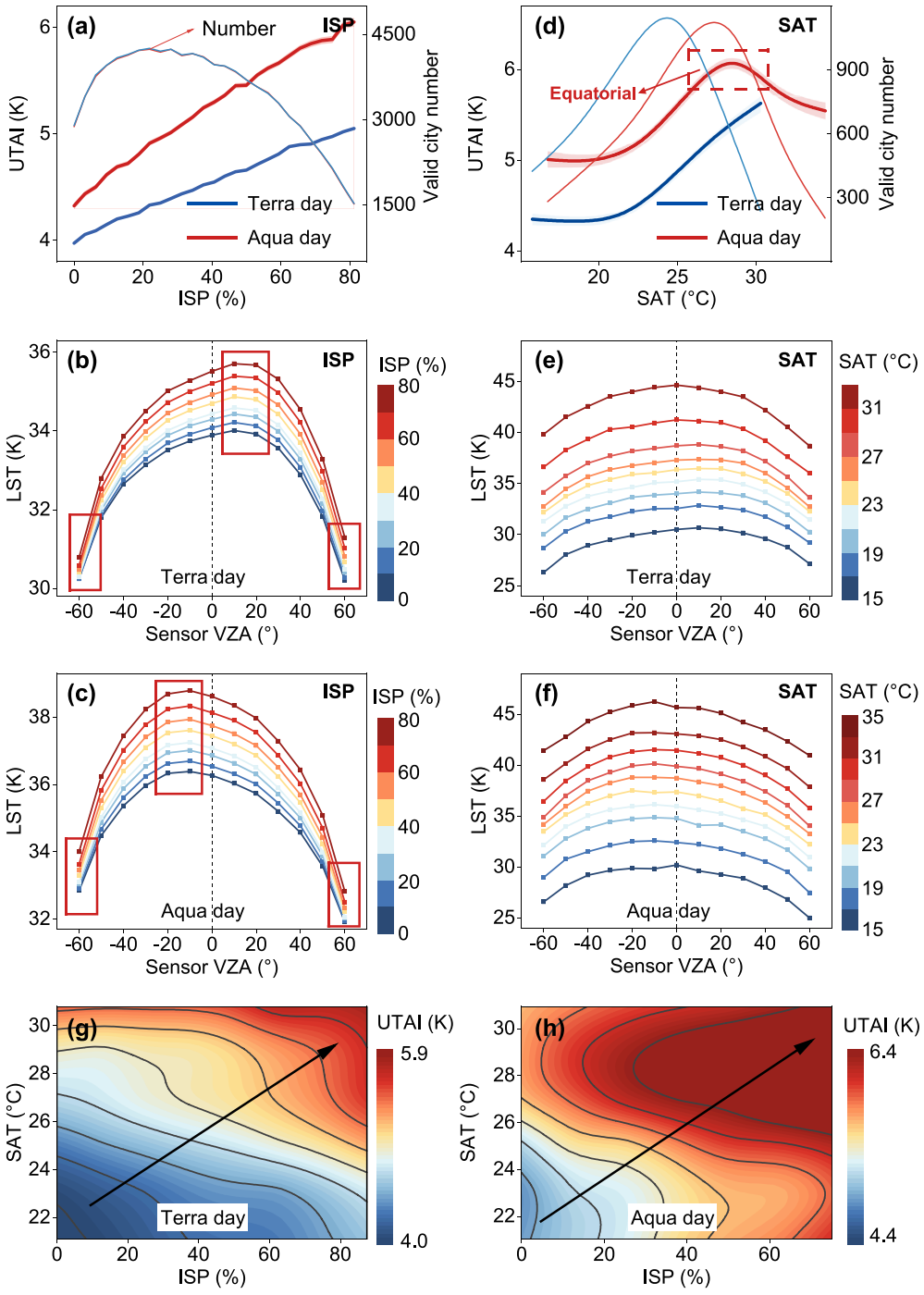

Fig. 5. Statistical relationships between the UTAI and several factors across global cities. The UTAI variations along with impervious surface percentage (ISP) (a) and surface air temperature (SAT) (d), the UTA curves with different ISPs for Terra day (b) and Aqua day (c) and with different SATs for Terra day (e) and Aqua day (f), and the UTAI variations jointly regulated by ISP and SAT for Terra day (g) and Aqua day (h).

3.4. Implications

By employing almost all available MODIS multi-angular LST observations, this study provides a first evaluation of UTA patterns across thousands of global cities with diverse contexts. Despite the potential UTAI underestimation due to our processing procedures (refer to Note S3 online), the results demonstrate that cities worldwide are characterized by notable UTA, especially during summer daytime (Fig. 2). We further show that UTA can substantially bias the estimates of satellite-retrieved urban climate variables, especially for urban surface sensible heat fluxes and surface urban heat island intensity (Fig. 3). However, practitioners can limit these biases within ±10% by using LSTs from sensor VZAs within ±30°.

Our results reveal that the global UTAI is highly associated with urban ISP and SAT (Fig. 5). This suggests the possibility of an empirical correction of instantaneous MODIS LSTs obtained from off-nadir angles to nadir across global cities. For instance, we can first construct the statistical relationships between LST corrections (i.e., the difference between off-nadir and nadir LST observations) and sensor VZA, ISP, and SAT at the global scale. For the practical

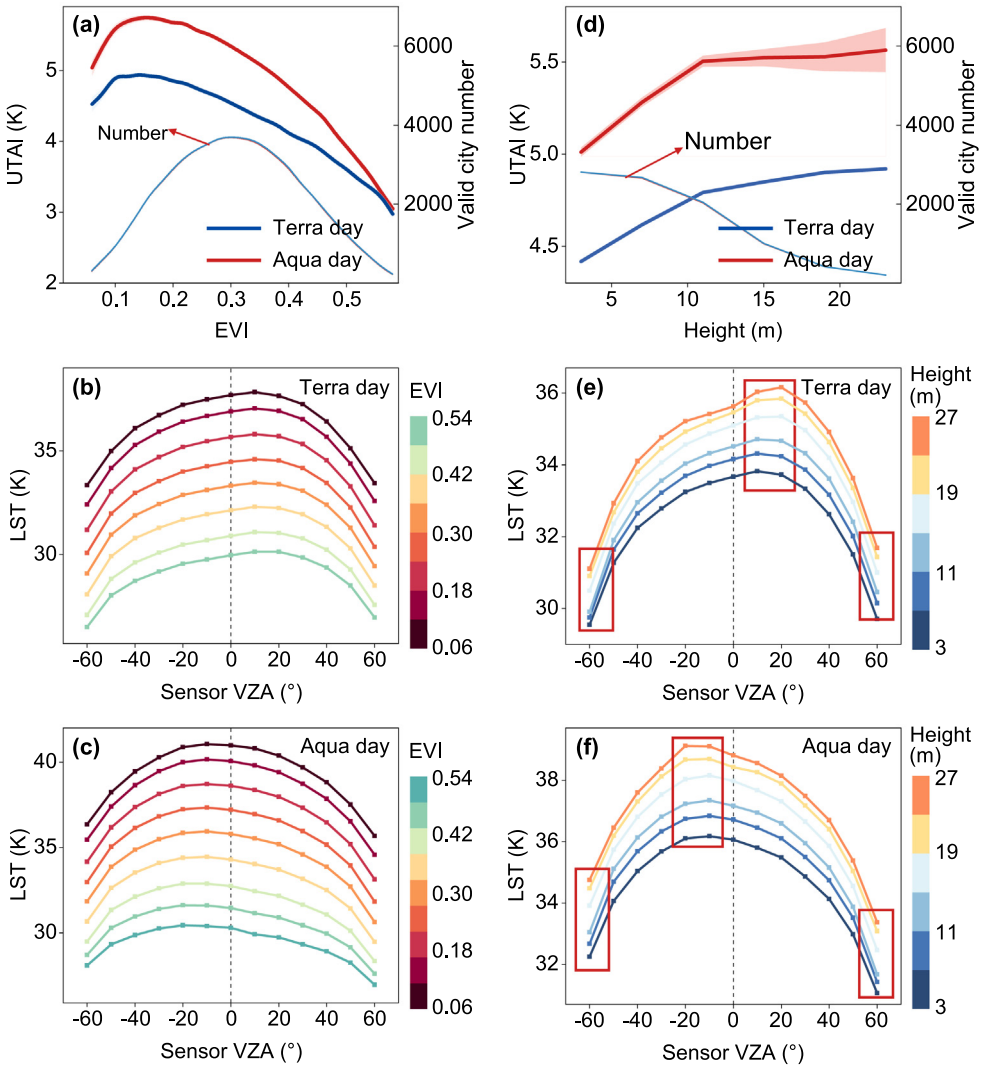

Fig. 6. Statistical relationships between the UTAI and several surface factors. The UTAI variations under different enhanced vegetation index (EVI; a) and building heights (d); and the UTA curves along with different EVIs for Terra day (b) and Aqua day (c) and with different building heights for Terra day (e) and Aqua day (f).

correction of slant LSTs for a specific city, the globally obtained statistical coefficients could then be adjusted by comparing the global mean UTAI and that of the specific city. These city-specific statistical coefficients can subsequently be applied toward the practical angular normalization of urban LST. Similarly, off-nadir urban LST can be normalized further to any other angle. By further incorporating the relationships between directional temperatures and hemispherical (or complete) temperatures, or other additional information from model simulations, it may be possible to obtain the hemispherical and even the complete urban LST that can better depict urban land surface–atmosphere interactions [46,47], or obtain the "incomplete" urban LSTs that are more relevant to practical applications such as human thermal comfort and building energy use [48]. We however need to emphasize that this study only investigates the UTA variations under different sensor VZAs by averaging all cases for solar zenith and azimuth angles. Future endeavors should further disentangle the multidimensional patterns of UTAI under different solar zenith angles, solar azimuth angles, sensor VZAs, and sensor azimuth angles within the entire hemisphere.

Conflict of interest

The authors declare that they have no conflict of interest.

Acknowledgments

We gratefully acknowledge the National Natural Science Foundation of China (42171306, 42001270, and 42201337) for providing support for this current study. We also thank the support from the National Youth Talent Support Program of China. TC Chakraborty's contribution was supported by Coastal Observations, Mechanisms, and Predictions Across Systems and Scales-Great Lakes Modeling (COMPASS-GLM), a multi-institutional project supported by the U.S. Department of Energy, Office of Science, Office of Biological and Environmental Research as part of the Earth and Environmental Systems Modeling program. Pacific Northwest National Laboratory is operated for the Department of Energy by Battelle Memorial Institute under contract DE-AC05-76RL01830. We would like to thank Dandan Wang from China University of Geosciences (Beijing) for providing thermal anisotropy results of

25 cities to assist comparative analysis, and to thank the anonymous reviewers for their insightful comments.

Author contributions

Wenfeng Zhan designed research; Huilin Du and Wenfeng Zhan performed data analysis; Huilin Du, Wenfeng Zhan, and Zihan Liu wrote manuscript; E. Scott Krayenhoff, TC Chakraborty, Lei Zhao, Lu Jiang, Pan Dong, Long Li, Fan Huang, Shasha Wang, and Yuyue Xu contributed ideas to data analysis, interpretation of results, or manuscript revisions.

Appendix A. Supplementary materials

Supplementary materials to this article can be found online at https://doi.org/10.1016/j.scib.2023.06.032.

References

[1] Grimm NB, Faeth SH, Golubiewski NE, et al. Global change and the ecology of cities. Science 2008;319:756–60.
[2] Krayenhoff ES, Moustaoui M, Broadbent AM, et al. Diurnal interaction between urban expansion, climate change and adaptation in US cities. Nat Clim Chang 2018;8:1097–103.
[3] Wang J, Chen Y, Liao WL, et al. Anthropogenic emissions and urbanization increase risk of compound hot extremes in cities. Nat Clim Chang 2021;11:1084–9.
[4] Zhao L, Lee XH, Smith RB, et al. Strong contributions of local background climate to urban heat islands. Nature 2014;511:216–9.
[5] Arnfield AJ. Two decades of urban climate research: a review of turbulence, exchanges of energy and water, and the urban heat island. Int J Climatol 2003;23:1–26.
[6] Oke TR, Mills G, Christen A, et al. Urban climates. Cambridge: Cambridge University Press; 2017.
[7] Stewart ID, Oke TR. Local climate zones for urban temperature studies. Bull Amer Meteorol Soc 2012;93:1879–900.
[8] Chakraborty T, Lee XH. A simplified urban-extent algorithm to characterize surface urban heat islands on a global scale and examine vegetation control on their spatiotemporal variability. Int J Appl Earth Obs Geoinf 2019;74:269–80.
[9] Li ZL, Tang BH, Wu H, et al. Satellite-derived land surface temperature: current status and perspectives. Remote Sens Environ 2013;131:14–37.
[10] Yang QQ, Huang X, Tang QH. Global assessment of the impact of irrigation on land surface temperature. Sci Bull 2020;65:1440–3.
[11] Hsu A, Sheriff G, Chakraborty T, et al. Disproportionate exposure to urban heat island intensity across major US cities. Nat Commun 2021;12:2721.
[12] Manoli G, Fatichi S, Schläpfer M, et al. Magnitude of urban heat islands largely explained by climate and population. Nature 2019;573:55–60.
[13] Voogt JA, Oke TR. Thermal remote sensing of urban climates. Remote Sens Environ 2003;86:370–84.
[14] Zhou DC, Xiao JF, Bonafoni S, et al. Satellite remote sensing of surface urban heat islands: progress, challenges, and perspectives. Remote Sens 2019;11:48.
[15] Roth M, Oke TR, Emery WJ. Satellite-derived urban heat islands from three coastal cities and the utilization of such data in urban climatology. Int J Remote Sens 1989;10:1699–720.
[16] Voogt JA, Oke TR. Effects of urban surface geometry on remotely-sensed surface temperature. Int J Remote Sens 1998;19:895–920.
[17] Lagouarde JP, Hénon A, Kurz B, et al. Modelling daytime thermal infrared directional anisotropy over Toulouse city centre. Remote Sens Environ 2010;114:87–105.
[18] Hu LQ, Monaghan A, Voogt JA, et al. A first satellite-based observational assessment of urban thermal anisotropy. Remote Sens Environ 2016;181:111–21.
[19] Manoli G, Fatichi S, Bou-Zeid E, et al. Seasonal hysteresis of surface urban heat islands. Proc Natl Acad Sci USA 2020;117:7082–9.
[20] Zhao L, Oleson K, Bou-Zeid E, et al. Global multi-model projections of local urban climates. Nat Clim Chang 2021;11:152–7.
[21] Jiang L, Zhan WF, Hu LQ, et al. Assessment of different kernel-driven models for daytime urban thermal radiation directionality simulation. Remote Sens Environ 2021;263:112562.
[22] Lagouarde JP, Irvine M. Directional anisotropy in thermal infrared measurements over Toulouse city centre during the CAPITOUL measurement campaigns: first results. Meteorol Atmos Phys 2008;102:173–85.
[23] Sugawara H, Takamura T. Longwave radiation flux from an urban canopy: evaluation via measurements of directional radiometric temperature. Remote Sens Environ 2006;104:226–37.
[24] Voogt JA, Grimmond C. Modeling surface sensible heat flux using surface radiative temperatures in a simple urban area. J Appl Meteorol Climatol 2000;39:1679–99.
[25] Wang DD, Chen YH, Hu LQ, et al. Satellite-based daytime urban thermal anisotropy: a comparison of 25 global cities. Remote Sens Environ 2022;283:113312.
[26] Wang DD, Chen YH, Hu LQ, et al. Urban thermal anisotropy: a comparison among observational and modeling approaches at different time scales. IEEE Trans Geosci Remote Sens 2022;60:1–15.
[27] Wang DD, Chen YH, Hu LQ, et al. Modeling the angular effect of MODIS LST in urban areas: a case study of Toulouse. France Remote Sens Environ 2021;257:112361.
[28] Hu LQ, Wendel J. Analysis of urban surface morphologic effects on diurnal thermal directional anisotropy. ISPRS-J Photogramm Remote Sens 2019;148:1–12.
[29] Krayenhoff ES, Voogt JA. Daytime thermal anisotropy of urban neighbourhoods: morphological causation. Remote Sens 2016;8:108.
[30] Wan ZM. Collection-6 MODIS land surface temperature products users' guide. Santa Barbara: Earth Research Institute, University of California; 2013.
[31] Friedl M, Sulla Menashe D. MCD12Q1 MODIS/Terra + Aqua Land Cover Type Yearly L3 Global 500 m SIN Grid V006. NASA EOSDIS Land Processes DAAC, 2019.
[32] Didan K, Munoz AB, Solano R, et al. MODIS vegetation index user's guide (MOD13 series). Tucson: Vegetation Index and Phenology Lab, University of Arizona, 2015. 35.
[33] Muñoz Sabater J. ERA5-land monthly averaged data from 1981 to present. Copernicus Clim Change Service Clim Data Store 2019;146:1999–2049.
[34] Li XC, Gong P, Zhou YY, et al. Mapping global urban boundaries from the global artificial impervious area (GAIA) data. Environ Res Lett 2020;15:094044.
[35] Pesaresi M, Ehrlich D, Ferri S, et al. Global human settlement analysis for disaster risk reduction. Int Arch Photogramm Remote Sens Spatial Inf Sci 2015;47:837–43.
[36] Li MM, Koks E, Taubenböck H, et al. Continental-scale mapping and analysis of 3D building structure. Remote Sens Environ 2020;245:111859.
[37] Pugachev VS. Probability theory and mathematical statistics for engineers. Amsterdam: Elsevier; 2014.
[38] Du HL, Zhan WF, Liu ZH, et al. Simultaneous investigation of surface and canopy urban heat islands over global cities. ISPRS-J Photogramm Remote Sens 2021;181:67–83.
[39] Hamdi R, Schayes G. Sensitivity study of the urban heat island intensity to urban characteristics. Int J Climatol 2008;28:973–82.
[40] Voogt JA. Assessment of an urban sensor view model for thermal anisotropy. Remote Sens Environ 2008;112:482–95.
[41] Gong P, Li XC, Wang J, et al. Annual maps of global artificial impervious area (GAIA) between 1985 and 2018. Remote Sens Environ 2020;236:111510.
[42] Ziter CD, Pedersen EJ, Kucharik CJ, et al. Scale-dependent interactions between tree canopy cover and impervious surfaces reduce daytime urban heat during summer. Proc Natl Acad Sci USA 2019;116:7575–80.
[43] Wang DD, Chen YH, Voogt JA, et al. An advanced geometric model to simulate thermal anisotropy time-series for simplified urban neighborhoods (GUTA-T). Remote Sens Environ 2020;237:111547.
[44] Dyce DR, Voogt JA. The influence of tree crowns on urban thermal effective anisotropy. Urban Clim 2018;23:91–113.
[45] Martilli A, Krayenhoff ES, Nazarian N. Is the urban heat island intensity relevant for heat mitigation studies? Urban Clim 2020;31:100541.
[46] Jiang L, Zhan WF, Voogt JA, et al. Remote estimation of complete urban surface temperature using only directional radiometric temperatures. Build Environ 2018;135:224–36.
[47] Voogt JA, Oke TR. Complete urban surface temperatures. J Appl Meteorol Climatol 1997;36:1117–32.
[48] Stewart ID, Krayenhoff ES, Voogt JA, et al. Time evolution of the surface urban heat island. Earth Future 2021; 9: e2021EF002178.

Huilin Du is now pursuing her doctorate degree at the International Institute for Earth System Science, Nanjing University. She received her B.S. and M.S. degrees from Taiyuan University of Technology and Nanjing University in 2019 and 2022, respectively. Her research primarily focuses on remote sensing of global urban heat islands.

Wenfeng Zhan is a professor at the International Institute for Earth System Science, Nanjing University. He received his B.S. degree in Wuhan University in 2007 and accomplished his Ph.D. degree in Beijing Normal University in 2012. He visited University of Western Ontario from 2010 to 2011 and Yale University from 2018 to 2019. He has worked extensively on the theories and applications of thermal remote sensing, with special focus on urban surfaces.

Zihan Liu is currently an assistant researcher at the International Institute for Earth System Science, Nanjing University. He received his doctor's degree in Geography at Nanjing University in 2021. His research mainly focuses on thermal remote sensing and its utilization in monitoring urban thermal environment.